COMPDYN 2015
5th ECCOMAS Thematic Conference on
Computational Methods in Structural Dynamics and Earthquake Engineering
M. Papadrakakis, V. Papadopoulos, V. Plevris (eds.)
Crete Island, Greece, 25–27 May 2015

ANISOTROPIC FAILURE CRITERION FOR BRITTLE MATERIALS USING ARTIFICIAL NEURAL NETWORKS

Vagelis Plevris[1] **and Panagiotis Asteris**[1]

[1] Computational Mechanics Laboratory, Department of Civil Engineering
School of Pedagogical & Technological Education
ASPETE Campus, Heraklion, GR 141 21, Athens, Greece
email: vplevris@aspete.gr, panagiotisasteris@gmail.com

Keywords: Anisotropy, brittle material, failure criterion, Artificial Neural Network.

Abstract. *Brittle materials are complex composite materials and a model is necessitated to realistically predict their load carrying capacity under any stress-state. During the last decades, a lot of failure criteria have been proposed for these materials in the literature. However, the majority of these models may substantially over-estimate the strength of the failure surface envelope. To overcome this problem a new approach is proposed which is based on Artificial Neural Networks (ANNs) techniques. The proposed approach is applied to a characteristic brittle anisotropic material such as the masonry material. The Neural Network managed to produce closed failure curves extending in all four quadrants of principal stresses, thus fully covering the compression and the tension stress areas. The comparison of the derived results with experimental findings demonstrates the promising potential of using ANNs for the reliable and robust approximation of the failure surface under biaxial stress state.*

1 INTRODUCTION

Despite the fact that masonry is one of the oldest structural materials and, actually, the main material of monumental structures such as churches, castles, mosques etc., our knowledge regarding its mechanical behavior is not as thorough as it should be and many aspects of its behavior remain to be investigated. Masonry exhibits distinct directional properties due to the influence of the mortar joints. Depending on the orientation of the joints to the stress directions, failure can occur in the joints alone or simultaneously in the joints and the blocks.

Nowadays, in developed societies, there is an increased interest about reliable and robust computational models for the modeling of masonry structures. This is primarily due to the growing interest of protecting heritage structures. The main characteristic of the majority of these structures is that they are mostly made of masonry. Taking into account the numerous uncertainties of the problem, a computational model, describing the masonry failure surface in a simple manner should be an efficient and useful tool for the investigation of the behavior of masonry structures.

To fulfill this need, in the last decades a large number of macro and micro computational models have been proposed for both the linear and the non-linear analysis of such structures [1-5]. Detailed and in-depth state-of-the-art reports can be found in [6-11]. The successful implementation of these advanced models requires reliable analytical constitutive rules such as constitutive equation models of masonry material failure. To date, research work has been focused on isotropic masonry models, which are based, primarily, on models applied for concrete. Regarding non-isotropic masonry, there are few research works in which failure criteria approximate the failure surface by employing different forms of quadratic polynomials. Many variations of such models have been published to date, including those defining the failure surface through the use of different functions for each quadrant [12-15]. However, for certain load cases, such models overestimate strength [16].

The present study applies Neural Networks in order to approximate the experimental failure curves of a brittle anisotropic material such as masonry. The aim of the study is to introduce an anisotropic (orthotropic) Neural Network – generated 3D failure surface under biaxial stress for masonry for any angle of the joints to the vertical compressive load, as described in detail in the following sections.

2 METHODOLOGY

The methodology of the present work is similar to another study by the authors [11], that focused only on the compression-compression area, where both principal stresses were compressive, i.e. it focused on the third quadrant of the σ_I-σ_{II} plane (compression-compression), without having to do with the other three quadrants. The present work continuous and extends that previous investigation to all four quadrants, namely the (A) tension-tension, (B) compression-tension, (C) compression-compression, and (D) tension-compression quadrant. This work utilizes the experimental data reported by Page [17-19], which have been also used by many other researchers [20, 21].

For all panels that were tested by Page [17-19], ratios of vertical compressive stress σ_I to horizontal compressive stress σ_{II} of 1, 2, 4, 10 and infinity (i.e. uniaxial σ_I) were used in conjunction with bed joint angle θ (with respect to σ_I) in directions of 0°, 22.5°, 45°, 67.5° and 90°. The pair cases (0°, 90°), (22.5°, 67.5°) are symmetric to each other. Principal stress ratios of 0 (i.e. uniaxial σ_{II}), 0.1, 0.25, 0.5 and 1 were obtained from the results using the symmetry of the panels and the loading. The failure envelopes that Page obtained by plotting mean curves for each bed joint angle can be found in Page [17-19] and [11]. These failure envelopes

are based on the peak strength values obtained from running bond masonry panel tests in which a uniform loading was applied proportionally. It should be emphasized that there are no real experimental data for the cases θ=67.5° and θ=90.0°, because these cases are equivalent to the cases θ=22.5° and θ=0.0°, respectively, if we reverse σ_I and σ_{II} stresses.

First, for each angle θ (0º, 22.5º, 45º, 67.5º, 90º) of the joints to the vertical compressive load, a Neural Network was trained with the experimental data of Page [17-19] as inputs (five NNs in total). Then each one of the five NNs was asked to produce the whole 2D failure curve (for each angle θ) as its output, filling also the gaps between the experimental points, thus "enriching" the experimental data with appropriate approximations. Then another, "global" NN was trained using the results of the five NNs as inputs with the angle θ as another input, also. The new NN was then asked to fill also the gaps between the angles θ, providing the whole 3D failure surface (a tube) for any angle θ (0º to 90º) and any ratio of σ_I/σ_{II}, for all four quadrants of stress.

3 BIAXIAL TESTING PROCEDURE

Masonry is a composite, multi-phase material that exhibits distinct brittle and strongly anisotropic behavior. The highly anisotropic brittle nature of masonry, renders complicated, difficult and expensive the realization of reliable experimental tests under conditions of biaxial stress, and, even more, under conditions of biaxial tension or heterogeneous stress. The angle of the applied loading to the bed joint plays a significant role in the behavior of the brick masonry discs. In general, the highest strength of masonry is observed when the compressive load is perpendicular to the bed joints or in other words when the principal tensile stress at the center of the disc is parallel to the bed joints. In this case, failure occurs through bricks and perpendicular joints. On the other hand, the lowest strength is observed when the compressive load is parallel to the bed joints or in other words when the principal tensile stress at the center of the disc is perpendicular to the bed joints. In this case failure occurs along the interface of brick and mortar joint.

In our study, in order to obtain the experimental results, a biaxial stress state is induced in the panel by loading with hydraulic jacks in two orthogonal directions. A constant load ratio is maintained during each test by means of the spreader beam. The load in each direction is monitored by load cells immediately adjacent to the specimen. Two main methodologies are used in the literature in order to obtain the final test specimens with the correct shape and size, presented in [22, 17-19, 23].

3.1 First methodology

Specimens with horizontal and vertical joints (Figure 1a) are constructed with dimensions greater than those of the final specimen, and then a square with the desired dimensions is drawn on the surface of the wall by a pencil at the appropriate orientation to achieve the correct lay-up angle as shown in Figure 1b, where the angle θ is the bed joint angle with respect to the horizontal direction.

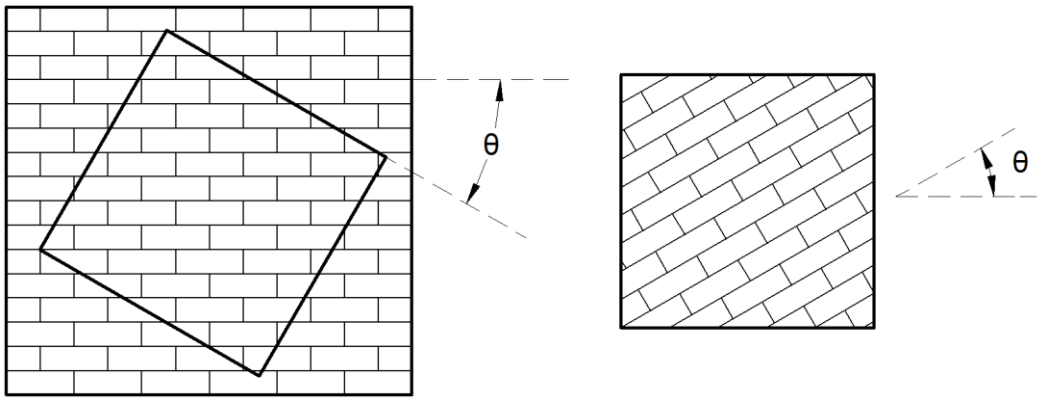

(a) (b)

Figure 1: Preparation of the masonry specimens.
(a) Wall panel before saw cut, (b) Saw cut specimen.

The lay-up angle is defined as the angle between the direction of the bed joints and one of the edges of the finished test specimen. Therefore, bed joints run at oblique incidence to the edges of the finished saw-cat specimen. After a time-span of 14 days the larger wall panels were cut to the required size and shape by a 'Clipper' saw. The 'Clipper' saw has the capacity to hold impregnated diamond edge circular blades of varying thickness and diameters. Two days prior to the date of testing, the 'compressive edge' of the panel (the side on which the compressive loads was to be applied) was capped with 1:1 (cement:sand) mortar [11].

3.2 Second methodology

According to Page [17-19] all specimens are constructed directly to their final shape and size as follows: All brickwork is constructed horizontally on a rigid form with bricks glued to a Perspex backing sheet to ensure a constant joint thickness. Panels are made with varying bed joint angles by cutting individual bricks to the required shape before casting. In the present study, five lay-up angles were selected for biaxial tests, namely 0°, 22.5°, 45°, 67.5° and 90°.

4 FIVE ARTIFICIAL NEURAL NETWORKS

In the present study, *Back-Propagation Neural Networks* (BPNNs) are used, in which the output values are compared with the correct answer to compute the value of a predefined error-function. The error is then fed back through the network. Using this information, the algorithm adjusts the weights of each connection in order to reduce the value of the error function by some small amount. The procedure is similar to the one used in a previous work by the authors [11], where more details can be found. The transfer function used in the present study is the hyperbolic tangent function, the same for all the hidden and the input layer, which yields output values in the interval [-1, 1], while its derivative yields output values in the interval [0, 1]. The transfer function for the output layer is a linear function. This scheme has been used for all the NNs of the study.

There are five NN models, one for each θ angle. For all five NNs, we used a BPNN with one hidden layer, one input layer and one output layer. The input layer had one node (neuron) which corresponds to the angle φ (in the range $[0, 2\pi]$), which defines the ratio σ_{II}/σ_{I}, while the output layer had also one node which corresponds to the distance (radius) r of the point on the failure curve to the origin of the axes. These two parameters (φ and r) will be described in detail in the next paragraphs. The hidden layer of each NN had 4 nodes for all θ (θ=0°, 22.5°,

45°, 67.5°, 90°), resulting in a 1-4-1 BPNN architecture for all five cases. These values have been chosen after some trial tests on various network architectures. The input and output values are normalized before the NN training and the inverse normalization is performed in order to obtain the NN results for other data, afterwards.

4.1 Preparation of the NN Input data

The experimental data of Page [17-19] have been used as inputs for the first five NN models of the present study.

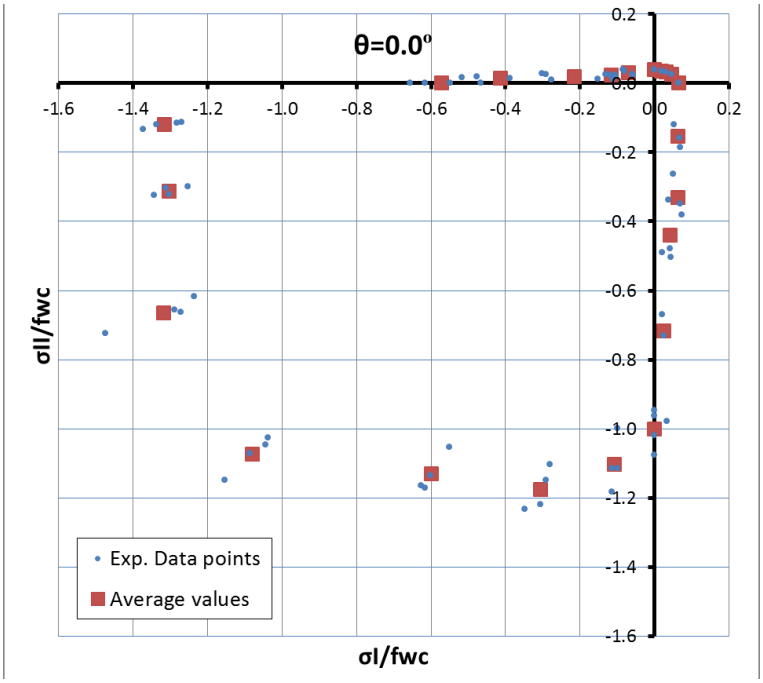

Figure 2: Normalized experimental data and average values for θ=0.0°.

The figure above shows the original data for the θ=0° case (in a normalized form, shown as blue points in the figure) together with the average values for each σ_I/σ_{II} ratio (shown as red squares). Table 1 shows the corresponding analytical data for the θ=0° case (average values for each test are shown only). The analytical data for the other θ cases are not reported in the present study.

The table consists of four parts, which correspond to four different types of tests, published in three different papers, as shown below:

A. 1st Quadrant: Biaxial Tension ($\sigma_I \geq 0$, $\sigma_{II} \geq 0$) [17]
B. 2nd Quadrant: Biaxial heterossemous Stresses (Compression – Tension) ($\sigma_I \leq 0$, $\sigma_{II} \geq 0$) [19]
C. 3rd Quadrant: Biaxial Compression ($\sigma_I \leq 0$, $\sigma_{II} \leq 0$) [18]
D. 4th Quadrant: Biaxial heterossemous Stresses (Tension – Compression) ($\sigma_I \geq 0$, $\sigma_{II} \leq 0$) [19]

Average σ_I/f_{wc}	Average σ_{II}/f_{wc}	Angle φ	Radius r	Region, Source
0.066	0.000	0.000	0.066	**A** Tension – Tension [17]
0.046	0.026	0.514	0.053	
0.032	0.032	0.784	0.045	
0.020	0.035	1.050	0.040	
0.000	0.038	1.571	0.038	
-0.070	0.031	2.731	0.077	**B** Compression – Tension [19]
-0.115	0.023	2.947	0.118	
-0.214	0.019	3.051	0.215	
-0.414	0.015	3.106	0.415	
-0.572	0.000	3.142	0.572	**C** Compression – Compression [18]
-1.316	-0.120	3.233	1.321	
-1.303	-0.312	3.377	1.340	
-1.318	-0.665	3.609	1.476	
-1.080	-1.073	3.924	1.522	
-0.599	-1.130	4.225	1.279	
-0.307	-1.175	4.457	1.215	
-0.107	-1.102	4.615	1.107	
0.000	-1.000	4.712	1.000	
0.025	-0.717	4.748	0.717	**D** Tension – Compression [19]
0.041	-0.440	4.806	0.442	
0.064	-0.331	4.904	0.337	
0.062	-0.154	5.097	0.166	

Table 1. Failure of Brickwork under Biaxial Compression, θ=0°.

The first two columns of the table contain the averages of the tests for each loading case, i.e. for each σ_{II}/σ_I ratio. The tension-tension experimental test (A) is the most difficult to perform and also the values are small and the data points more dense, so there is only one test for every σ_{II}/σ_I ratio, while for Parts B, C, D we have 2, 3 or 4 tests for each case. As a result, for Part A, the average values coincide with the values themselves, as there is only one test performed for each σ_{II}/σ_I ratio. The data are in a dimensionless form where the stresses have been divided with the stress f_{wc} which is the masonry strength for the case $\sigma_I=0$ for Case C (Compression – Compression case). The value of f_{wc} has been calculated as the average of the four values corresponding to four tests (7.15, 7.27, 7.69, 8.12) as 7.56 MPa.

For the data to be suitable for the Neural Network training, a conversion to polar coordinates (r, φ) is needed, where the distance (or radius, Column 4 of the table) r is given by

$$r = \sqrt{\sigma_{I,aver}{}^2 + \sigma_{II,aver}{}^2} \tag{1}$$

where $\sigma_{I,aver}$ and $\sigma_{II,aver}$ are the average stresses for each loading case (columns 1, 2). Since we are trying to describe a full circle, the polar angle value φ has to be within $[0, 2\pi)$ range. Based on the values of σ_I and σ_{II}, we need to calculate the value of the polar angle φ. For Part A (Tension-Tension), this can be done easily using the Inverse Tangent function (Arctan) as follows:

$$\varphi_A = \mathrm{Arc}\tan\left(\frac{\sigma_{II}}{\sigma_I}\right) \tag{2}$$

The Arctan function always returns values within the (-π, π) range. In the last case of Part A, it is $\sigma_I=0$ and as a result Eq. (2) cannot be defined. In this case it is obviously $\varphi=\pi/2$. The range of φ_A is [0, π/2].

For Part B (2nd quadrant) it is $\sigma_I\leq 0$, $\sigma_{II}\geq 0$, while for Part C (3rd quadrant) it is $\sigma_I\leq 0$, $\sigma_{II}\leq 0$. In these two cases, in order to get the value of φ, the following formula hat to be used:

$$\varphi_B = \varphi_C = \pi + \text{Arc tan}\left(\frac{\sigma_{II}}{\sigma_I}\right) \tag{3}$$

In the last case of Part C, it is $\sigma_I=0$ and as a result Eq. (2) cannot be defined. In this case it is obviously $\varphi=3\pi/2$. The range of φ_B is [π/2, π] and the range of φ_C is [π, 3π/2].

For Part D (4th quadrant) it is $\sigma_I\geq 0$, $\sigma_{II}\leq 0$. In this case, the following formula is applicable:

$$\varphi_D = 2\pi + \text{Arc tan}\left(\frac{\sigma_{II}}{\sigma_I}\right) \tag{4}$$

Angle φ is given in Column 3 of the table. The figures below show the corresponding diagrams for the other two main θ cases (θ=22.5°, θ=45°). The other two cases, θ=67.5° and θ=90° are omitted here, as they are symmetric to the cases θ=22.5°, θ=45°), respectively. The symmetry is about the line $\sigma_I=\sigma_{II}$.

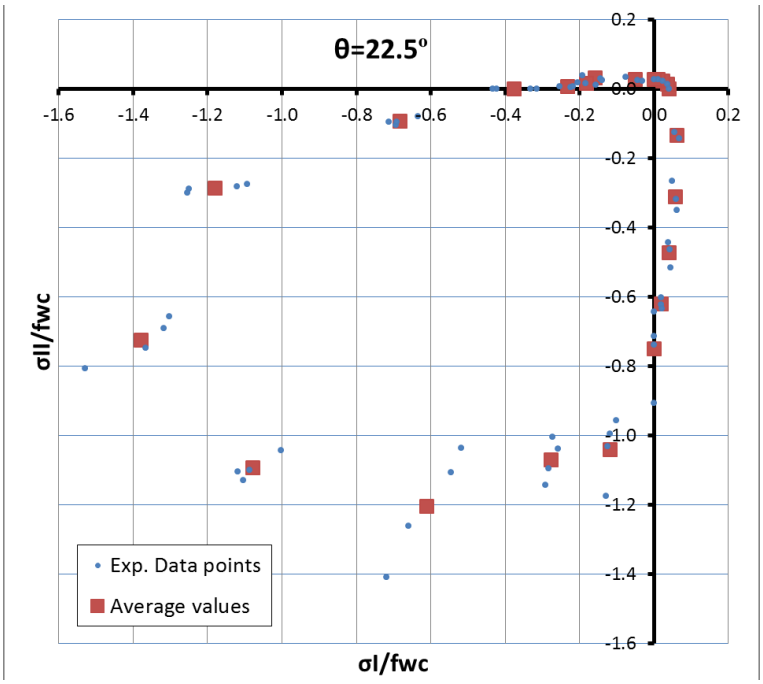

Figure 3: Normalized experimental data and average values for θ=22.5°.

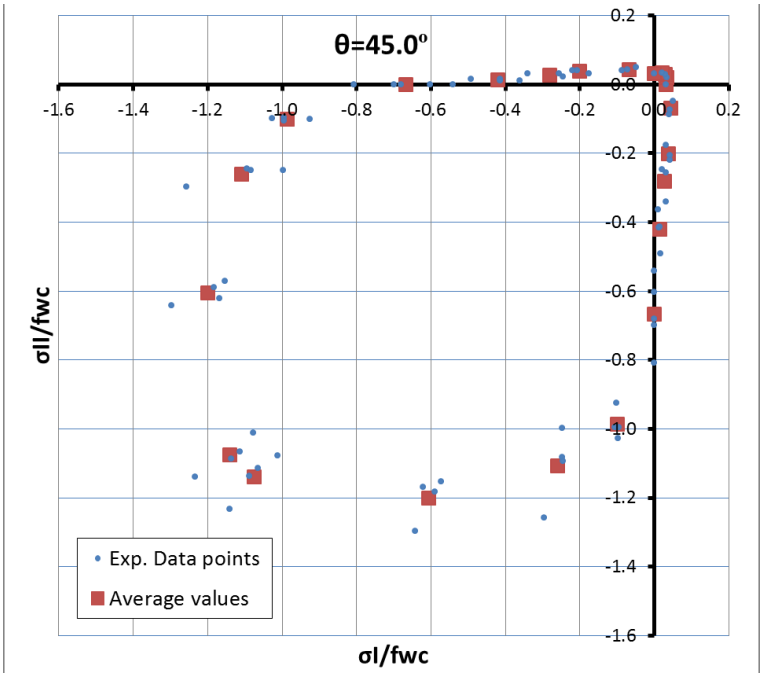

Figure 4: Normalized experimental data and average values for θ=45.0°.

The data (and also the failure curve itself) for θ=45° are symmetric with respect to the 45° diagonal line (σ_I=σ_{II}), due to not only the nature of the loading but also to the geometry of the masonry panel where for this special case the bed joint orientation is equal to angle θ=45°. The data for θ=0° and θ=90° that correspond to complementary angles are also mutually symmetric to the line σ_I=σ_{II}. The same also applies for the data for θ=22.5° and θ=67.5. These special conditions will be studied in detail in the next paragraphs.

For each of the five angles θ (θ=0°, 22.5°, 45°, 67.5°, 90°), a separate Neural Network is trained with the angle φ as its input and the radius r as its output. It should be noted that only the average values of each test (denoted as "square" points in the above figures) are used as training data for the Neural Networks.

4.2 Properties of the curves - NN Corrections

The failure curves have some distinct characteristics and the NN results need to be in some cases corrected in order to comply and exactly follow the rules. These characteristics are mentioned below.

1. *Consistency for φ=0 and φ=2π.* The case φ=0 (start of circle) is in fact the same case as φ=2π (end of circle) and the results in these two points (start and end of circle) should coincide.
2. *Symmetry for θ=45°.* For the special case of masonry with bed joint angle θ=45°, the masonry panel exhibits a symmetry which leads to a symmetric failure curve (to the line σ_I=σ_{II}).
3. *Symmetry for any complementary angles (θ and 90°-θ).* The failure curves that correspond to complementary angles (θ and 90°-θ), such as θ=0° and θ=90° as well as θ=22.5° and θ=67.5°, are mutually symmetric to the line σ_I=σ_{II}.

Although the results obtained by the NNs are in most cases very satisfactory in their original form, we apply some special corrections in order to ensure that the above rules are satisfied with 100% accuracy.

For point (1) of the above, we take into account two full identical cycles of data when training the NN. This means that instead of stopping at $\varphi=2\pi$, the NN is trained for two cycles of data, until $\varphi=4\pi$. Also, a correction is applied in order to ensure that the result (radius r) will be exactly the same for $\varphi=0$ and $\varphi=2\pi$.

For points (2) and (3), when a symmetric result is expected, we take into account the average values between the two symmetric cases and this way we apply the correction. This technique is applied in the $\theta=45°$ case itself and also for the mutually symmetric cases ($\theta=0°$, $\theta=90°$) as well as ($\theta=22.5°$, $\theta=67.5°$). In particular, the results of the two equivalent cases are both taken into account and the average is finally considered, ensuring that the result would be perfectly symmetric between the two cases. The symmetry is to the line $\sigma_I=\sigma_{II}$ for all cases.

4.3 Final approximation results of the five NNs

The five NNs were trained with the input and output data and then each NN was asked to produce the full curves for each bed joint angle, for a set of 80 segments (81 points). Although each NN was trained for two circles of data, it was asked to report results only for the first circle (in th

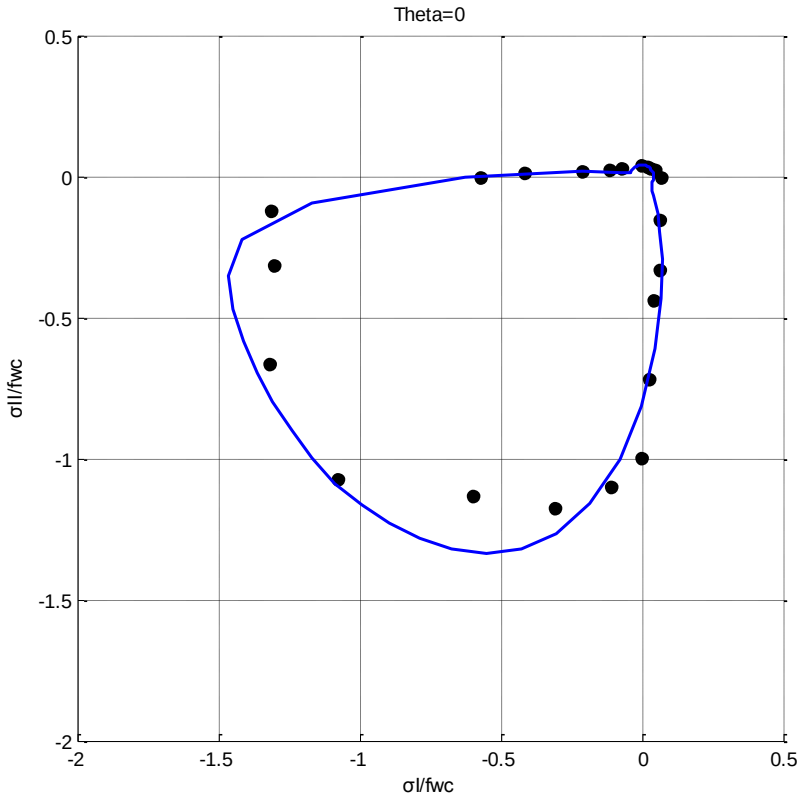

Figure 5: NN approximation result for θ=0°.

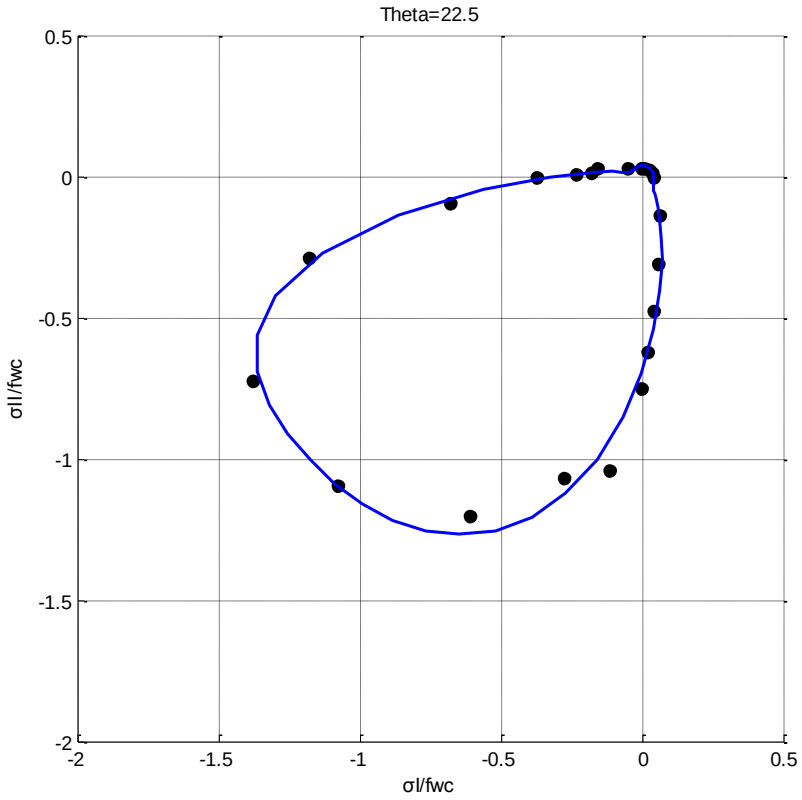

Figure 6: NN approximation result for θ=22.5°

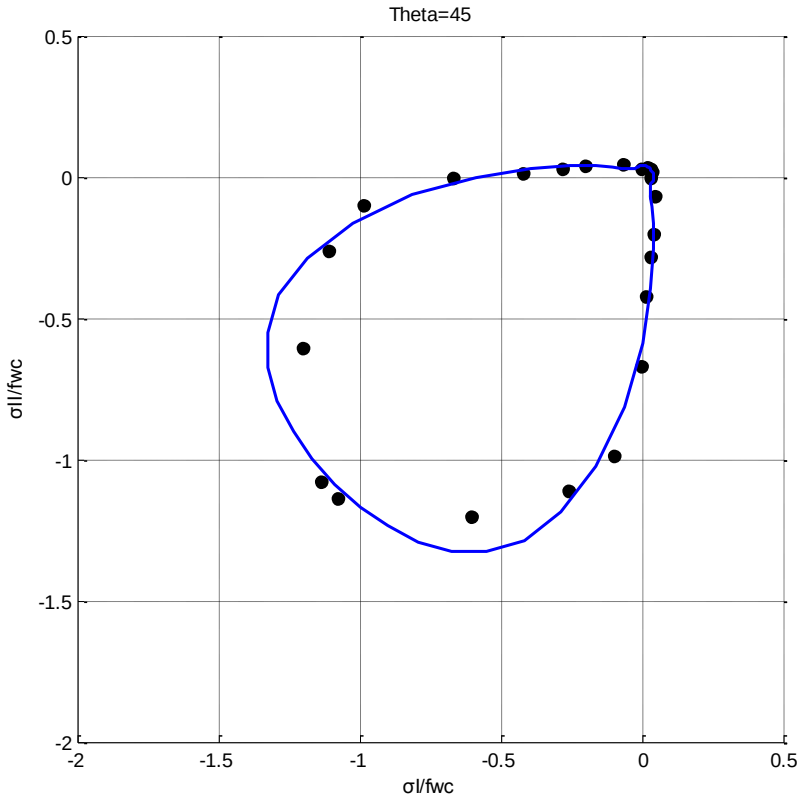

Figure 7: NN approximation result for θ=45°.

In all the above figures, the black dots denote the input data, i.e. the data corresponding to columns 3, 4 of the table. The blue curve denotes the NN prediction of the failure curve. It can be seen that the NN managed to fit all the training data with very good accuracy, providing smooth curves in all cases. For the θ=45° case, it can be seen that the curve is perfectly symmetric to the σ_I=σ_{II} line, due to the extra measures that have been taken.

5 "GLOBAL" NN MODEL AND RESULTS

Five NN Models were trained, each for one angle θ (0°, 22.5°, 45°, 67.5° and 90°). The final purpose of the study is to add also the angle θ as a parameter of the problem, thus create a model that will be able to predict the entire failure curve not only for the predefined angles, but for any angle θ, from 0° to 90°. In order to achieve this, after the five NNs were trained and they had provided their results, another "Global" NN was also trained which took the results of the five NNs as inputs with the angle θ as an additional input, also. The new NN was then asked to fill the gaps between the angles θ, providing the whole 3D failure "tube" for any angle θ and any angle φ (i.e. ratio of σ_{II}/σ_I), for all four stress quadrants.

The Global NN is a BPNN with one hidden layer containing 10 nodes (2-10-1 architecture). The two inputs are the angles φ (0 to 4π - two full circles) and θ (0° to 90°), while the output is the distance (radius) r. The transfer function of the global NN is the hyperbolic tangent function. For the global NN, we use all the results of the previous five NNs as training patterns. This means that we have 161*5 = 805 training patterns, as we use 161 points (80*2+1) for every angle θ (0°, 22.5°, 45°, 67.5° and 90°).

The global NN was trained and then asked to produce the whole 3D failure surface. Although the global NN was trained in two full circles ([0, 4π]), in order to achieve better performance and to manage to "close" the curve for the first circle, it was asked to produce results only for the first circle ([0, 2π]). Specifically, the NN was asked to produce points where the angle φ was divided again in 160 (80*2) segments (161 points, each segment is equivalent to 360°/80=4.5°), while angle θ is divided in 40 segments (41 points, each segment is equivalent to 90°/40=2.25°). The figure below shows the result of the NN approximation in 3D (two different views of the tube). The red points (dots) denote the initial training set of the first five NNs, i.e. the average values gathered from the experimental results and used for the training of the NNs.

6 CONCLUSIONS

In the last decades, there have been many attempts on modeling the materials' constitutive rules by means of Neural Networks. However there have not been many attempts to apply a Neural Network (NN) for the prediction of masonry behavior in general. In the present paper, following and expanding a previous work by the authors [10] which focused on biaxial compressive stress only, the use of Neural Networks is proposed to approximate the failure surface of masonry materials in a dimensionless form for any quadrant of stress state.

A novel procedure based on Neural Networks techniques has been introduced in order to model the failure/yield surface of masonry material in dimensionless form. Available classical experimental results from the literature are used as inputs for the training of the NN. The proposed NN procedure is demonstrated and has been shown to be reliable and robust.

The derived failure surface fits the experimental data with excellent accuracy, while it is in dimensionless form which is very important in order to be able to be applied for every masonry material. Furthermore, the derived surface can provide valuable information about areas of the masonry failure that have not been investigated until now (failure under heterosemous

stresses or failure under biaxial tension for any tilt angle of the bed joints) helping us better understand the phenomena involved in fracture mechanics.

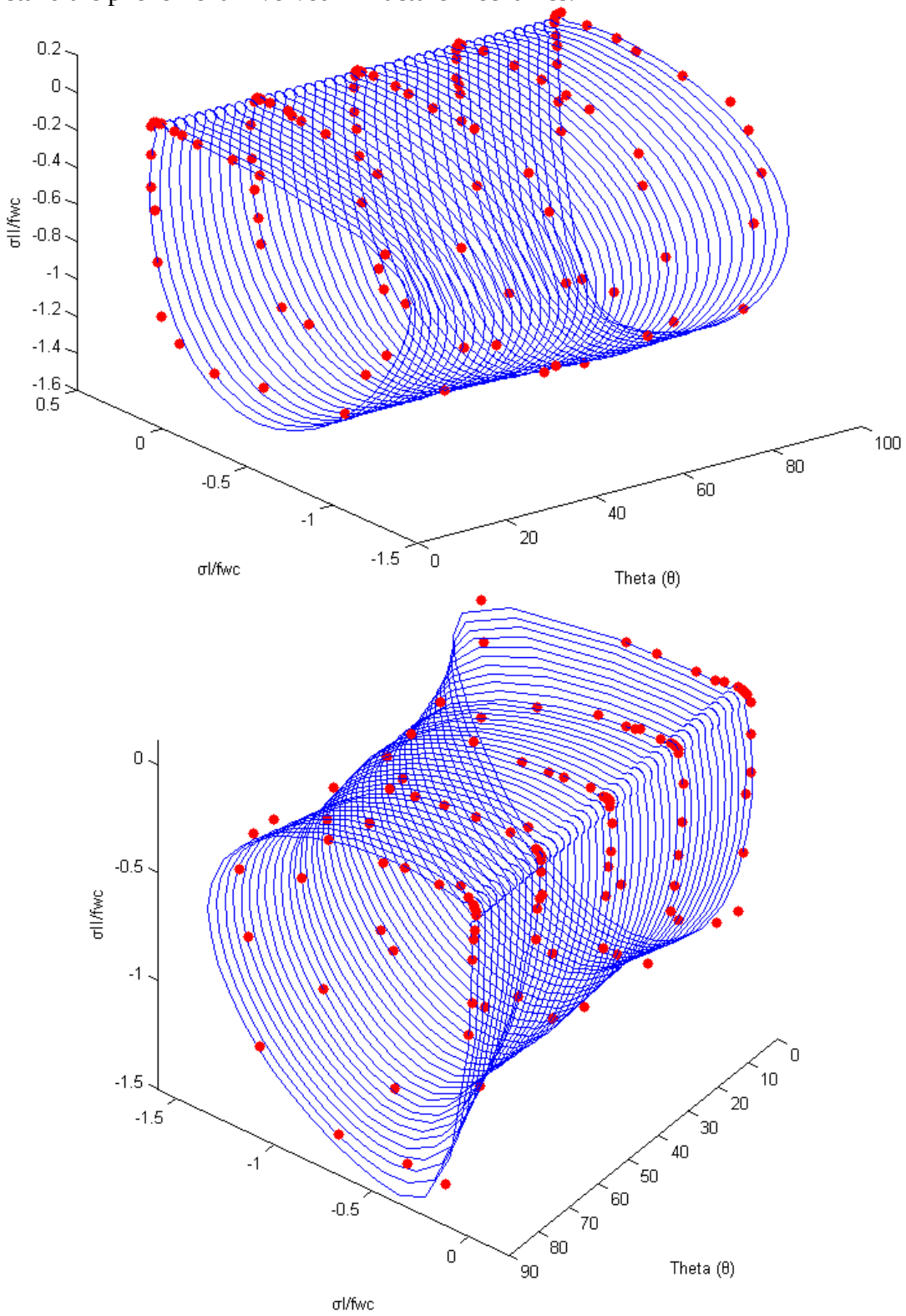

Figure 8: Global NN approximation result of the 3D failure surface in terms of principal stresses

(two different views of the failure tube.

REFERENCES

[1] Lourenço, P.B., Rots, J.G. and Blaauwendraad, J. (1998). Continuum model for masonry: parameter estimation and validation, Journal of Structural Engineering, 124(6), pp.642-652.

[2] Caliò I., Marletta M. and Pantò B. (2012). A new discrete element model for the evaluation of the seismic behavior of unreinforced masonry buildings, Engineering Structures, 40, pp. 327-338.

[3] Penna, A., Lagomarsino, S., Galasco, A. (2014). A nonlinear macroelement model for the seismic analysis of masonry buildings, Earthquake Engineering and Structural Dynamics, 43(2), pp. 159-179.

[4] Asteris, P.G., Chronopoulos, M.P., Chrysostomou, C.Z., Varum, H., Plevris, V., Kyriakides, N., Silva, V. (2014). Seismic vulnerability assessment of historical masonry structural systems, Engineering Structures, Volume 62-63, 15 March 2014, Pages 118-134

[5] Reccia, E., Milani, G., Cecchi, A., Tralli, A. (2014). Full 3D homogenization approach to investigate the behavior of masonry arch bridges: The Venice trans-lagoon railway bridge, Construction and Building Materials, 66, 567-586.

[6] Lourenço, P.B. (2002). Computations on historic masonry structures, Progress in Structural Engineering and Materials, 4(3), pp. 301-319.

[7] Roca, P., Cervera, M., Gariup, G. and Pela, L. (2010). Structural analysis of masonry historical constructions. Classical and advanced approaches, Archives of Computational Methods in Engineering, 17(3), pp. 299-325.

[8] Asteris, P.G., Antoniou, S.T., Sophianopoulos, D.S., Chrysostomou, C.Z. (2011). Mathematical macromodeling of infilled frames: State of the art, Journal of Structural Engineering, 137 (12), pp. 1508-1517

[9] Sarhosis V. (2012). Computational modelling of low bond strength masonry. Phd thesis. University of Leeds, UK

[10] Asteris, P.G., Cotsovos, D.M., Chrysostomou, C.Z.,Mohebkhah, A., Al-Chaar, G.K. (2013). Mathematical micromodeling of infilled frames: State of the art, Engineering Structures, 56, pp. 1905-1921

[11] Plevris, V., Asteris, P.G. (2014). Modeling of masonry failure surface under biaxial compressive stress using Neural Networks, Construction and Building Materials, 55, pp. 447-461

[12] Ganz, H.R. (1989). Failure criteria for masonry, Proc. of the 5th Canadian Masonry Symposium, pp. 65-77

[13] Lourenço, P.B., De Borst, R., Rots, J.G. (1997). Plane stress softening plasticity model for orthotropic materials. Int J Numer Methods Eng, 40:4033–57.

[14] Massart, T.J., Peerlings, R.H.J., Geers, M.G.D., Gottcheiner, S. (2005). Mesoscopic modeling of failure in brick masonry accounting for three-dimensional effects, Engineering Fracture Mechanics, 72 (8), pp. 1238-1253

[15] Pelà, L., Cervera, M., Roca, P. (2013). An orthotropic damage model for the analysis of masonry structures, Construction and Building Materials, 41, pp. 957-967

[16] Tsai, S.W., Wu, E.M. (1971). A general failure criterion for anisotropic materials. Journal of Composite Materials 1971; 5: 58-80

[17] Page, A. W. (1980), "A biaxial failure criterion for brick masonry in the tension-tension range." The International journal of Masonry Construction, Vol. 1, No. 1.

[18] Page, A. W. (1981), "The biaxial compressive strength of brick masonry", Proc. Instn Civ. Engrs, Part 2, Vol. 71, Sept., 893-906, 1981.

[19] Page, A. W. (1983). The strength of brick masonry under biaxial tension-compression, International Journal of Masonry Construction, 3(1), 26-31.

[20] Duan, Z.H., S.C. Kou, C.S. Poon, Using artificial neural networks for predicting the elastic modulus of recycled aggregate concrete, Construction and Building Materials 44 (2013) 524–532

[21] Naraine, K., and Sinha, S., "Cyclic Behavior of Brick Masonry under Biaxial Compression." Journal of Structural Engineering, ASCE, Vol. 117, No. 5, 1336-1355, 1991.

[22] Samarasinghe, W., "The in-plane failure of brickwork," PhD thesis, University of Edinburgh, 1980.

[23] Tassios, Th. P., and Vachliotis, Ch. (1989). ''Failure of masonry under heterosemous biaxial stresses.'' Proc., Int. Conf. Conservation of Stone, Masonry—Diagnosis, Repair and Strengthening, Athens.